Triggering apoptosis in cancer cells with an analogue of cribrostatin 6 that elevates intracellular ROS.

D. J. Asby,[†,a] M. G. Radigois,[†,a,b] D. C. Wilson,[a] F. Cuda,[a] C. L. L. Chai,[b,c] A. Chen,[b] A. S. Bienemann,[d] M. E. Light,[a] D. C. Harrowven,[*,a] and A. Tavassoli[*,a,e]

[a]Chemistry, University of Southampton, Southampton, SO17 1BJ, UK.
[b]Institute of Chemical and Engineering Sciences, A*Star, Singapore, 138665.
[c]Department of Pharmacy, National University of Singapore, Singapore, 117543.
[d]School of Clinical Sciences, University of Bristol, Southmead Hospital, Bristol, BS10 5NB, UK.
[e]The Institute for Life Sciences, University of Southampton, Southampton, UK.
† Authors contributed equally
*e-mail: dch2@soton.ac.uk and ali1@soton.ac.uk

Elevation of reactive oxygen species (ROS) is both a consequence and driver of the upregulated metabolism and proliferation of transformed cells. The resulting increase in oxidative stress is postulated to saturate the cellular antioxidant machinery, leaving cancer cells susceptible to agents that further elevate their intracellular oxidative stress. Several small molecules, including the marine natural product cribrostatin 6, have been demonstrated to trigger apoptosis in cancer cells by increasing intracellular ROS. Here, we report the modular synthesis of a series of cribrostatin 6 derivatives, and assessment of their activity in a number of cell lines. We establish that placing a phenyl ring on carbon 8 of cribrostatin leads to increase potency, and observe a window of selectivity towards cancer cells. The mechanism of activity of this more potent analogue is assessed and demonstrated to induce apoptosis in cancer cells by increasing ROS. Our results demonstrate the potential for targeting tumors with molecules that enhance intracellular oxidative stress.

Aerobic glycolysis is a key characteristic of cancer cells that significantly affects the metabolic pathways and metabolites of transformed cells. While these changes enable the unregulated growth and survival of cancer cells, they may also be used for selective chemotherapeutic targeting. One such defining change is the increased production of ROS and the subsequent additional oxidative stress placed on cancer cells (1), which is thought to be play a key role in the maintenance of the tumour phenotype (2-4). Adaptation to this increase in oxidative stress requires upregulation of the cellular antioxidant machinery, which works to maintain the reducing environment necessary for correct function of a variety of cellular processes (5). NADPH and glutathione are key antioxidants whose levels are elevated in response to increased ROS. The

antioxidant machinery of cancer cells is thought to operate at near capacity due to higher basal ROS and upregulated ROS-mediated signalling, which potentially makes them vulnerable to agents that cause additional oxidative pressure, providing a mechanism by which cancer cells can be selectively targeted (6). In line with this hypothesis, a range of chemotherapeutics have been proposed to function by increasing the oxidative stress in cancer cells (7-10), and several screens aimed at identifying compounds that selectively inhibit the growth of transformed cells have converged on compounds that act to increase oxidative pressure by reducing glutathione levels (11-13). Compounds such as phenyl isocyanate (12), 2-methoxyoestradiol (14), and piperlongumine (11) selectively kill cancer cells (at doses of 5-20 μM) by interfering with ROS homeostasis pathways.

Cribrostatin 6 is an imidazo[5,1-a]isoquinoline isolated from the marine sponge Cribrochalina sp (15), which has been shown to be cytotoxic in several cancer cell lines, triggering apoptosis by elevating intracellular ROS (16). The mechanism of this process is likely to be similar to other quinones, which undergo bioreduction in cells to the corresponding semiquinone, which then reacts with molecular oxygen to generate superoxide (8). Cancer cells treated with cribrostatin 6 also showed an elevation of antioxidant transcripts, including heme oxygenase 1, several ferritins and proteins associated with glutathione synthesis (16). Although cribrostatin 6 has been shown to affect the viability of cancer cell lines, its selectivity for cancer cells over normal cells has never been demonstrated. Such selectivity is seldom explored, yet is increasingly seen as a critical property of compounds proposed as potential cancer therapeutics. Given its mechanism of action and the demonstrated susceptibility of cancer cells to additional oxidative stress, we sought to generate a more potent analogue of cribrostatin 6, with the aim of improving both the potency and cancer cell selectivity.

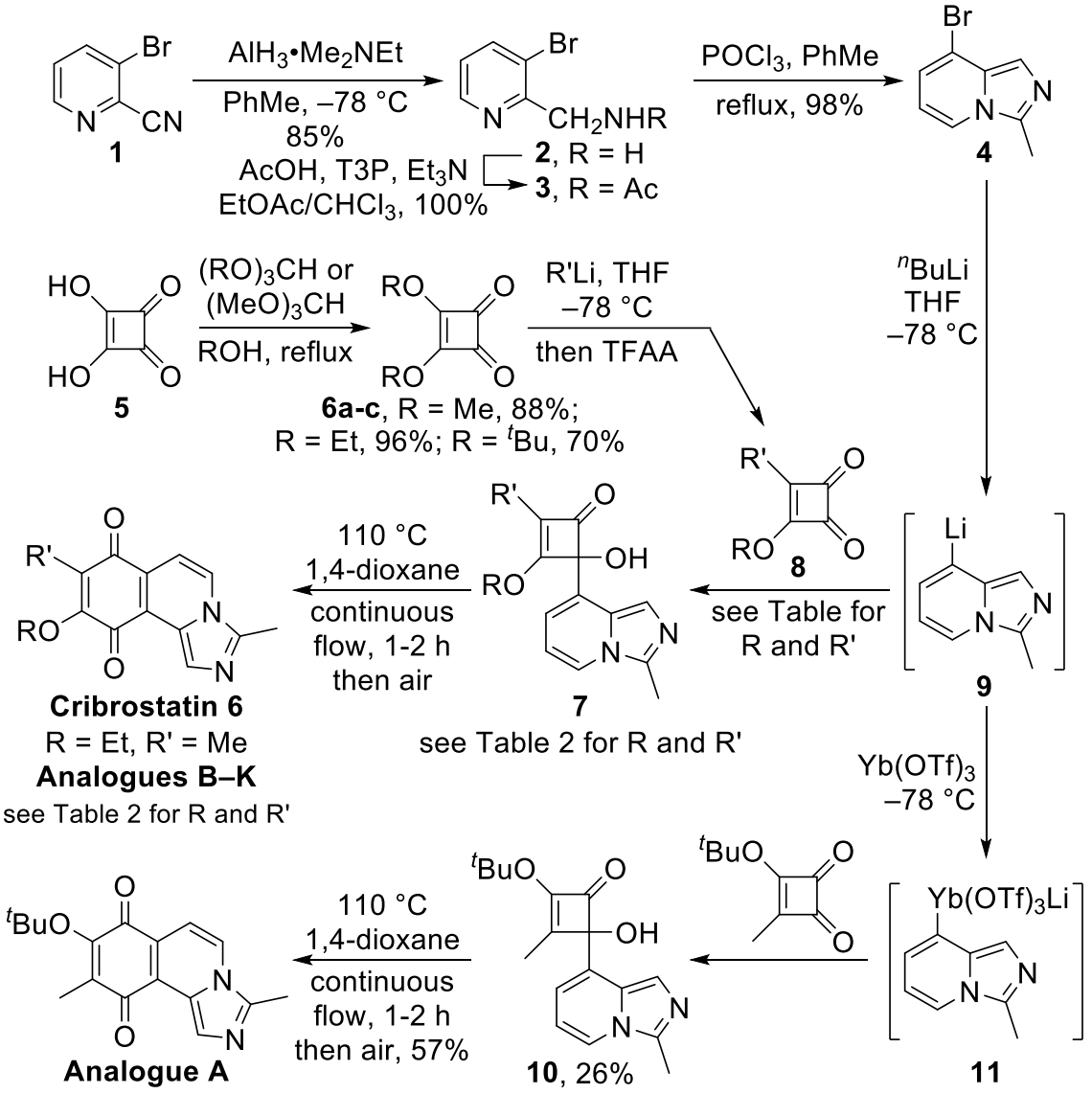

Scheme 1. Synthesis of cribrostatin 6 and analogues A-K.

There have been several reported total syntheses of cribrostatin 6 (17-21). We chose to adapt a modular route that we had developed as it facilitated the rapid incorporation of a variety of substituents on carbons 8 and 9 of the isoquinoline ring and was readily adapted to reverse the positioning of these alkyl and alkoxy residues (Scheme 1) (20). Thus, the brominated core, imidazo[1,5-a]pyridine **4**, was prepared in three steps from 3-bromo-2-cyanopyridine **1** as previously described (20). Contemporaneously, a series of cyclobutenediones **8** were prepared as surrogates for the quinone ring each bearing alkoxy and organyl residues at C3 and C4 respectively. Syntheses of cribrostatin 6 and analogues B–K were then achieved by halogen–lithium exchange of **4**, addition of the resulting aryllithium **9** to a cyclobutenedione **8** and thermolysis of the resulting adduct **7** with aerial oxidation. To achieve a synthesis of analogue A, in which the positions of the alkyl and alkoxy residues are swapped, required a subtle change of strategy. In this

case the simple expedient of switching from organolithium intermediate **9** to organoytterbium ate complex **11** changed the course of nucleophilic addition in favor of addition to the vinylogous ester carbonyl C3 (22). Thermolysis of the resulting adduct **10** followed by aerial oxidation then gave analogue A.

The effect of cribrostatin 6 and analogues A–K on the viability of MCF7 breast cancer cells was measured by MTT (3-(4,5-dimethylthiazol-2-yl)-2,5-diphenyltetrazolium bromide) assay (Table 1 and Supplementary Figure 1-12). The most potent molecule was analogue D (IC_{50} of 428 ± 40 nM) with a phenyl ring on C8 in place of the methyl residue found in the parent molecule (Figure 1A, from hereon referred to as 8PC6, for 8-phenylcribrostatin 6). This substitution resulted in a 30% increase in potency against MCF7 breast cancer cells compared to cribrostatin 6 (IC_{50} of 628 ± 67 nM).

Table 1. The effect of cribrostatin 6 and its synthetic analogues on the viability of MCF7 breast cancer cells. R and R' refer to structures in Scheme 1.

Compound	R	R'	IC_{50} (nM)
Cribrostatin 6	OEt	Me	628 ± 67
Analogue A	Me	O^{t}Bu	2064 ± 884
Analogue B	O^{t}Bu	Me	1546 ± 243
Analogue C	OEt	^{t}Bu	1671 ± 112
Analogue D	OEt	Ph	428 ± 40
Analogue E	OEt	Naphthyl	2024 ± 329
Analogue F	OEt	2,4,6-$(OMe)_3$Ph	1692 ± 209
Analogue G	OEt	4-(Me_3Si)Ph	5064 ± 2766
Analogue H	OEt	4-(Me)Ph	993 ± 160
Analogue I	OEt	4-(F_3C)Ph	1661 ± 230
Analogue J	OEt	4-(Me_3C)Ph	4275 ± 1358
Analogue K	OEt	4-(2-furanyl)	2393 ± 476

With a more potent analogue in hand, we assessed the effect of 1 μM 8PC6 on a number of cancer and non-cancer cell lines from a variety of tissue types (Figure 1B). As a comparison, we also assessed the effect of 1 μM cribrostatin 6 in the same panel of cells (Figure 1). 8PC6 was more potent than cribrostatin 6 in all cases, with a greater effect on the viability of the cancer cell lines (reduced to 16-28%) than normal cells (reduced to 69-88%). The selectivity of cribrostatin 6 for the cancer cell lines in our panel (reduced to 36-54%) over normal cells (viability reduced to 69-87%) was less pronounced at this dose (Figure 1).

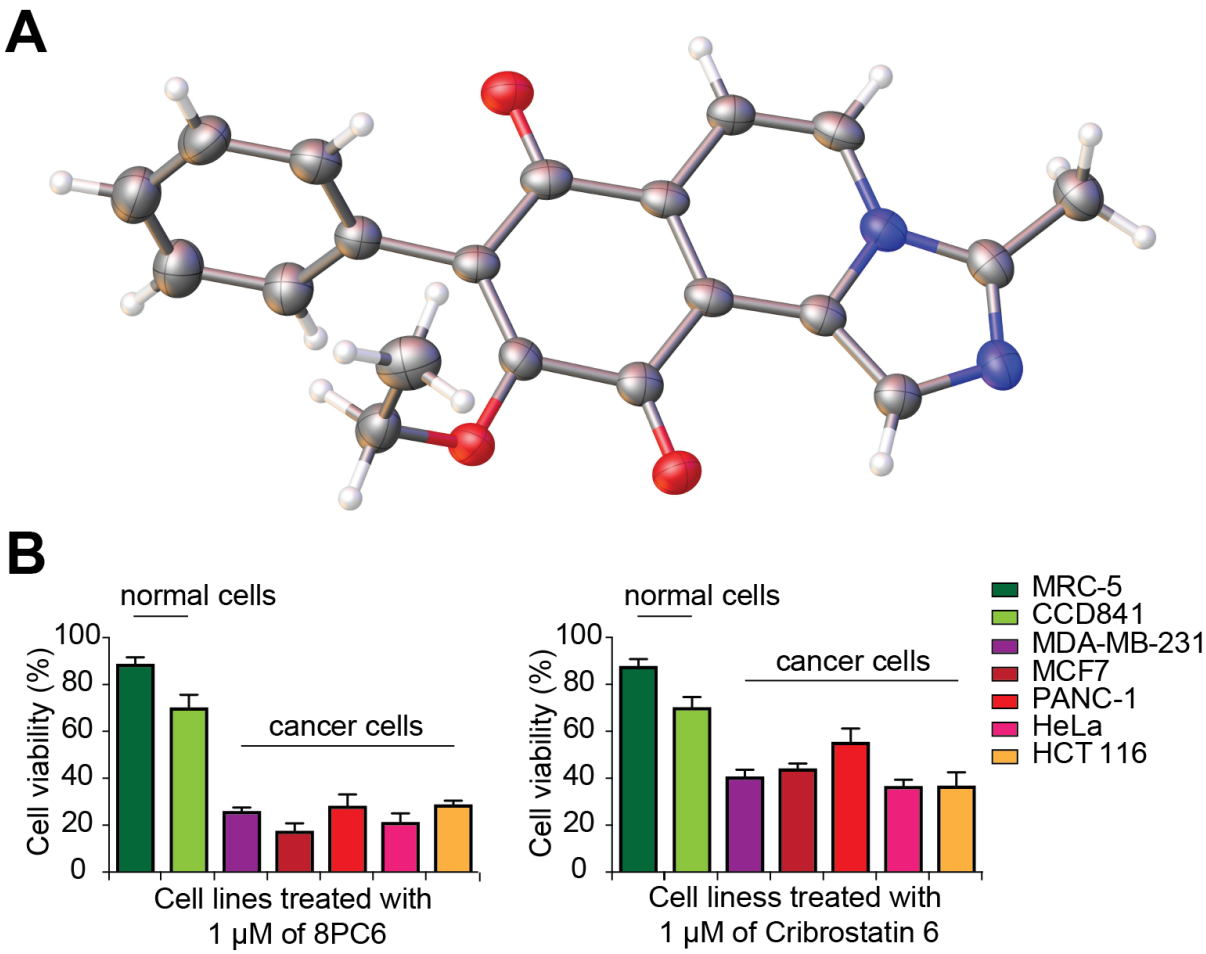

Figure 1. Selective inhibition of cancer cell viability by cribrostatin 6 and 8PC6. A) the crystal structure of 8P6C (CCDC deposition code 1060587). **B)** The effect of 1 μM cribrostatin 6 and 8PC6 on the viability of a panel of cancer and non-cancer cell lines.

Table 2. The effect of 8PC6 and cribrostatin 6 on the viability of a variety of cell lines

Cell line	Tissue and type	8PC6 IC_{50} (nM)	Cribrostatin 6 IC_{50} (nM)
MRC-5	Lung, normal	1845 ± 186	2231 ± 173
CCD841	Colon, normal	1798 ± 429	2189 ± 587
MDA-MB-231	Breast, adenocarcinoma	502 ± 76	726 ± 99
MCF7	Breast, adenocarcinoma	428 ± 40	628 ± 67
PANC-1	Pancreas, epithelioid carcinoma	505 ± 55	1045 ± 212
HeLa	Cervix, adenocarcinoma	418 ± 36	659 ± 51
HCT 116	Colon, colorectal carcinoma	548 ± 69	748 ± 75

The IC_{50} of 8PC6 was next determined by MTT assay in each of these cell lines (Table 2, and Supplementary Figure 20-26). The IC_{50} of 8PC6 was found to be ca. four-fold higher in non-cancer cell lines (average IC_{50} of 1.8 μM) than that in cancer cell lines

(average IC_{50} of 480 nM). In addition, 8PC6 was more potent than its parent molecule in every cell line (Table 2).

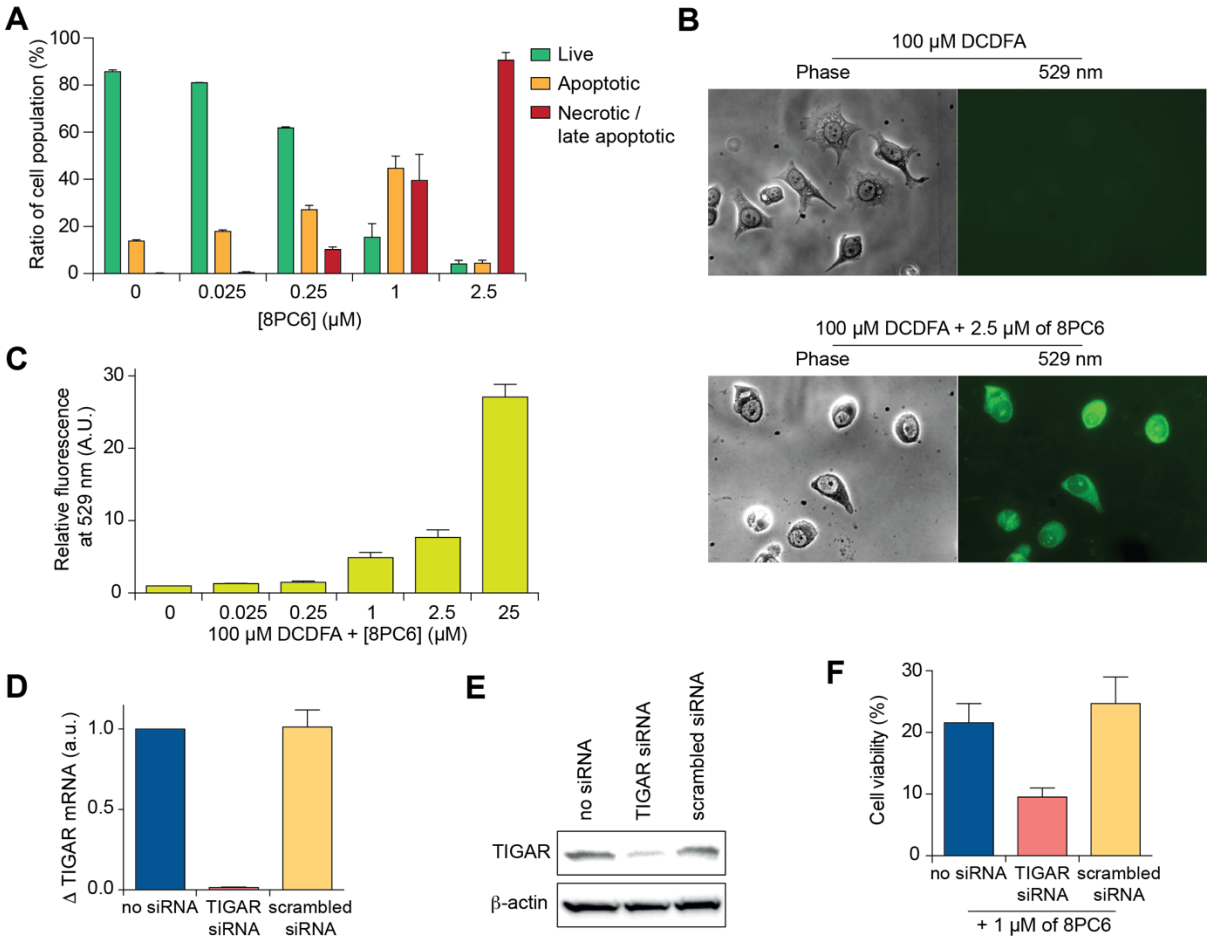

Figure 2. The effect of 8PC6 on intracellular ROS, and the effect of increased intracellular ROS on the potency of 8PC6. A) Flow cytometric analysis of the effect of 8PC6 treatment on the cell population by annexin V and 7-aminoactinomycin staining and flow cytometry. For scatter plots see Supplementary Figure 27. B) Phase and fluorescent micrographs of MCF7 cells treated with 100 μM DCDFA (upper panel), and MCF7 cells dosed with 100 μM DCDFA followed by 2.5 μM 8PC6 (lower panel). Intracellular ROS causes DCDFA to be Fluorescent at 529 nm. C) Quantifying the increase in the fluorescence (at 529 nm) of MCF7 cells treated with 100 μM DCDFA and increasing doses of 8PC6. D) The effect of TIGAR and scrambled siRNA on TIGAR mRNA in MCF7 cells. E) The effect of TIGAR and scrambled siRNA on TIGAR protein in MCF7 cells. F) Knockdown of TIGAR increases the potency of 8PC6 by 2-fold in MCF7 cells.

We next sought to determine the mechanism of cell death induced by 8PC6. Flow cytometry was used to assess annexin V and 7-aminoactinomycin D staining in cells treated with increasing doses of 8PC6 (25 nM–2.5 μM) for 24 hours (Figure 2A and Supplementary Figure 27). In cells treated with <1 μM 8PC6 we observed a dose-dependent increase in cells undergoing the earlier stages of apoptosis, accompanied

by a reduction in cell viability, and a small percentage of late apoptotic and/or necrotic cells (Figure 2A). At doses higher than 1μM of 8PC6, we observed a much greater proportion of cells in the latter stages of apoptosis, accompanied by a reduction in the number of cells expressing phosphotidylserine and very low levels of total cell viability (Figure 2A). The observed pattern of annexin V/7-AAD staining for 8PC6 is indicative of cell death via apoptosis and agrees with previously reported data for cribrostatin 6 (16).

The effect of 8PC6 on intracellular ROS levels was next probed using the ROS-sensing dye 2',7'-dichlorofluorescin diacetate (DCFDA) (3, 23). No fluorescence was observed at 529 nm in MCF7 cells treated with 100 μM DCFDA alone (Figure 2B, upper panel), whereas a significant increase in 529 nm fluorescence was observed when cells were treated with 2.5 μM 8PC6 prior to the addition of 100 μM DCFDA (Figure 2B, lower panel). Quantification of this change in fluorescence showed a dose-dependent increase in fluorescence with increasing doses of 8PC6 (Figure 2C), indicating that treatment with 8PC6 results in an increase in intracellular ROS.

These data suggest that 8PC6 selectively targets cancer cells, presumably as a result of their increased ROS content. Consequently, we next sought to establish a link between variations in intracellular ROS and the effect of 8PC6 on cell viability in the same cell line. To increase intracellular ROS we utilized TIGAR, a P53-inducible protein that regulates glycolysis and apoptosis and serves to protect cells from ROS. Knockdown of TIGAR has been shown to result in an increase in intracellular ROS (24), therefore the effect of 8PC6 would be expected to be more pronounced in cells treated with TIGAR siRNA. MCF7 cells treated with 50 nM TIGAR siRNA showed the expected knockdown in TIGAR mRNA and protein levels, while 50 nM of scrambled control siRNA had no effect on TIGAR mRNA or protein levels (Figure 2D and 2E). In line with our hypothesis, 1 μM of 8PC6 reduced the viability of MCF7 cells with TIGAR knocked-down by over 90%, a 2-fold increase in potency compared to the effect of the same dose of 8PC6 in untreated MCF7 cells and/or MCF7 cells treated with scrambled siRNA (Figure 2F). The effect of TIGAR knockdown on the IC_{50} of 8PC6 was further quantified; the IC_{50} of 8PC6 was 478 ± 76 nM in untreated MCF7 cells and 477 ± 150 nM in MCF7 cells treated with scrambled siRNA, whereas the potency of 8PC6 was increased by 1.5-fold, with an IC_{50} of 326 ± 19 nM, in MCF7 cells treated with TIGAR siRNA (Supplementary Figure 28-30).

To assess the effect of 8PC6 in MCF7 cells with reduced intracellular ROS we utilized *N*-acetylcysteine (NAC), a molecule that not only functions as a ROS-scavenger, but also acts as the precursor to glutathione (another ROS-scavenging molecule) (25). NAC-treatment has previously been shown to protect cells from the oxidative damage

of other ROS-generating molecules (11), and would therefore be expected to reduce the effect of 8PC6 on cancer cell viability. The protective effect of NAC was apparent when comparing micrographs of MCF7 cells pre-treated with NAC prior to administration of 8PC6, to those treated with 8PC6 only (Figure 3A). The observed protective effect of NAC on 8PC6-treated cells was quantified by MTT assay; pre-treatment of MCF7 cells with 5mM NAC resulted in a 20-fold loss in the potency of 8PC6, with the IC_{50} of 8PC6 increasing to 9086 ± 95 nM in these cells (Figure 3B). The above data demonstrates that the activity and potency of 8PC6 directly correlates with intracellular ROS levels.

The mechanism of action of 8PC6 was next probed. The generation of superoxide by quinones requires molecular oxygen (8), and as 8PC6 is proposed to function through a similar mechanism, its potency is expected to be reduced in cells pre-incubated in a hypoxic environment. It should be noted that while hypoxia leads to a short-term increase in basal ROS in cells (6, 26), the decrease in molecular oxygen levels within these cells means that ROS generation by 8PC6 and its subsequent effect on cell viability would be expected to be reduced.

MCF7 cells were pre-incubated in hypoxia for 24 hours, treated with increasing doses of 8PC6 in hypoxia, and the effect on cell viability measured by MTT assay after a further 24h of incubation in a hypoxic environment. In line with our hypothesis, the IC_{50} of 8PC6 was significantly raised in hypoxic MCF7 cells to 19.6 ± 7 μM (Figure 3C). To further demonstrate the link between the observed loss of 8PC6 potency in hypoxia and the reduction in molecular oxygen, MCF7 cells were pre-incubated in hypoxia, treated with 8PC6 and then switched to a normoxic environment for 24 h prior to assessing their viability by MTT assay. The IC_{50} of 8PC6 was measured as 1.47 ± 0.1 μM in these cells. This increase in the potency of 8PC6 (compared to cells treated and incubated in hypoxia only) demonstrates the necessity of molecular oxygen for the activity of this 8PC6.

The effect of 8PC6 on the long-term proliferative potential of cancer cells was probed using a colony forming assay. MCF7 cells were treated with a single dose of 8PC6 (0.5 μM, 1 μM, 1.5 μM, 2 μM) and incubated for 10 days to assess their colony forming potential. We observed a dose-dependent reduction in the number and size of colonies formed in cells treated with 8PC6 compared to untreated cells (Figure 3D and Supplementary Figure 30), with a 2 μM dose of 8PC6 causing a 2.7-fold reduction in the clonogenicity of MCF7 cells (Supplementary Figure 31).

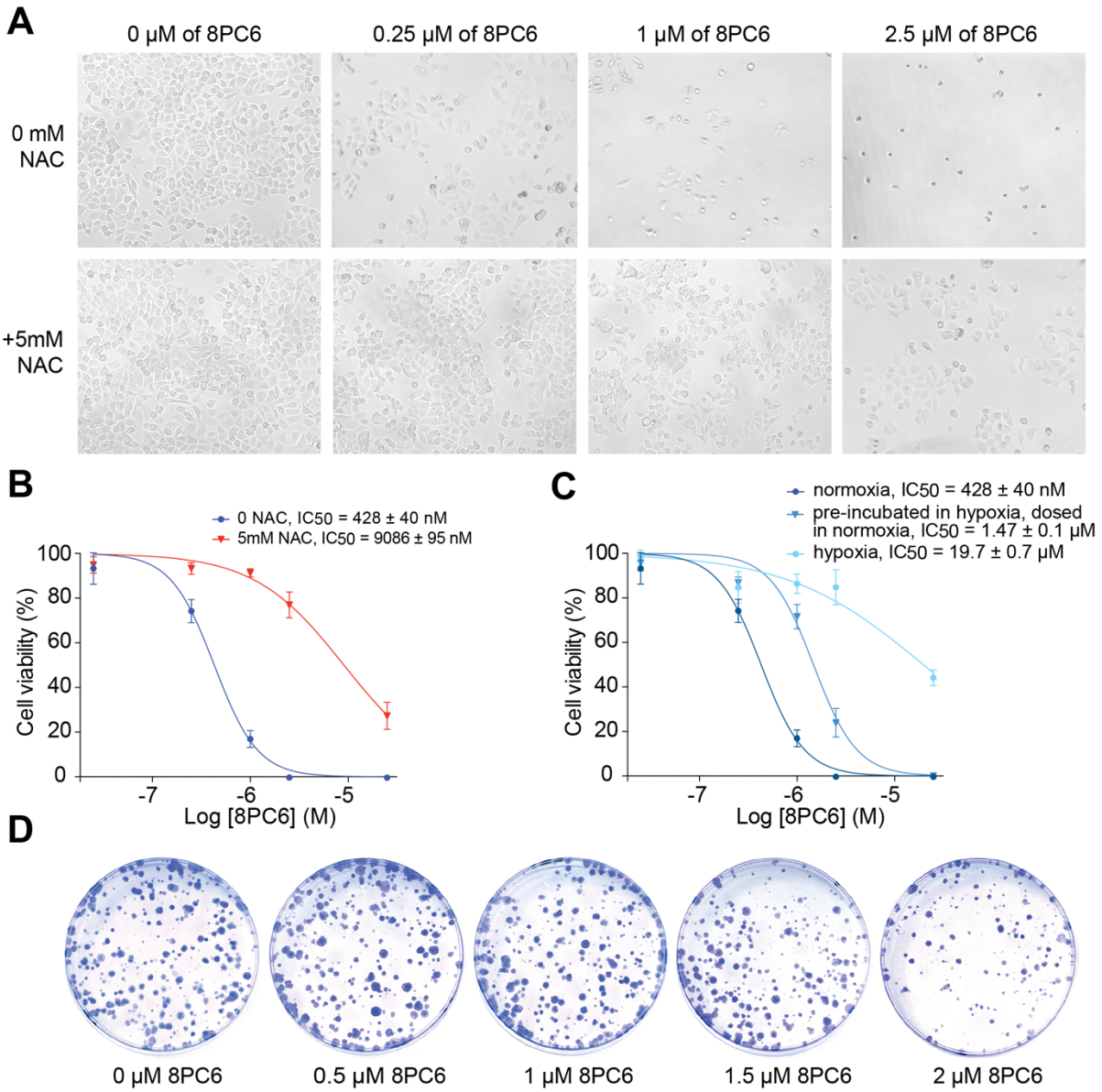

Figure 3. Probing the role of 8PC6 in MCF7 cells. A) Micrographs of MCF7 cells treated with increasing doses of 8PC6 (top row) and MCF7 cells treated with 5 mM NAC prior to dosing with 8PC6 (bottom row). B) The effect of 5 mM of NAC on the potency of 8PC6 in MCF7 cells. C) The effect of a hypoxic microenvironment of the potency of 8PC6. D) The effect of increasing doses of 8PC6 on the clonogenic survival of MCF7 cells (quantified in Supplementary Figure 31).

Conclusions

Our findings demonstrate that 8PC6 and cribrostatin 6 selectively inhibit the growth of cancer cells via elevation of intracellular ROS. Work is currently underway in our laboratories to further probe the mechanism and effect of 8PC6 in other cell lines, and we are continuing to synthesize and assess additional derivatives of this molecule.

Materials and Methods

Synthetic chemistry

Please see supplementary materials and methods for detailed experimental procedures and spectroscopic data for all molecules synthesized.

Cell treatments

Cells were grown in the presence or absence of test compounds for 24 hours unless stated otherwise. For all compounds, serially diluted stock solutions were made up in DMSO and then further diluted such that the final concentration of DMSO in each well was 0.5% v/v. For treatment with N-acetylcysteine (NAC), an aqueous solution of NAC was added to cells for 1 h prior to addition of 8PC6, with a final concentration of NAC of 5 mM. For experiments involving the culture of cells under hypoxic conditions, cells were initially cultured and seeded under normoxic conditions, and then transferred to a hypoxia workstation (H35 Hypoxystation, Don Whitley) and either pre-incubated for 24 h in hypoxic conditions (1% oxygen, 5% carbon dioxide, 37^{o}C) and then dosed and incubated with 8PC6 in normoxic conditions for 24 h; or grown continuously in hypoxic conditions, including 24 h of pre-incubation and 24 h of treatment with 8PC6.

MTT cell viability assays

Cells were seeded in triplicate in 96-well plates at optimized cell densities appropriate to the size and doubling times of the various cell lines used in the study to produce equivalent cell confluency prior to experiments (MCF-7 8000 cells / well; HeLa 6000 cells / well; PANC-1 10,000 cells / well; MDA-MB-231 12,000 cells / well; HCT116 20,000 cells / well; MRC5 6000 cells / well; and CCD841 7000 cells / well). Cells were incubated for 16 hours prior to dosing with test compounds in fresh medium. MTT-based cell proliferation assays were performed 24 hours post-dosing, as follows: culture medium was replaced with fresh culture medium without phenol red. 3-(4,5-dimethylthiazol-2-yl)-2,5-diphenyl tetrazolium bromide (MTT; Sigma) was freshly prepared in sterile PBS and added to cells at a final concentration of 1 mM (10% v/v). Cells were then incubated for up to 4 hours at 37^{o}C until intracellular punctate purple precipitates were clearly visible under the microscope. An equal volume of DMSO was then added to solubilize the resulting formazan and the cells incubated for 5 minutes in the dark at room temperature with agitation to further dissolve the insoluble formazan particles. Absorbance was measured at 570 nm on a microplate reader (Tecan Infinite M200 Pro) and corrected for 650 nm background. Each well was triplicated and each experiment repeated at least three times. IC50 values quoted are mean ± SEM.

Detection of ROS species using DCF-DA fluorophore

MCF-7 cells were either seeded in duplicate at 20,000 MCF-7 cells per well in collagen-coated 8-well NUNC LabTek 2 chamber slides for fluorescent microscopy or seeded in triplicate at 10,000 MCF-7 cells per well in a black 96-well plate for quantitative fluorescent assays. In both cases cells were then incubated for 16 hours in cell culture media without phenol red prior to any treatments. Culture media was gently removed, and the cells washed in warm PBS. Warm PBS containing dichlorodihydrofluorescein diacetate (DCF-DA, Sigma) was added to the cells to give a final concentration of 100 μM, and the cells were incubated for 30min with the dye. The PBS containing DCF-DA was then gently removed, and replaced with fresh cell culture media without phenol red. Cells were then dosed with 8PC6 and incubated for 6 hours. For the fluorescent microscopy experiments, cells on chamber slides were imaged using a fluorescent microscope (Ex 495nm / Em 529nm) and the experiment was repeated three times with representative micrographs shown. For quantitative analyses of DCF-DA fluorescence, cells on black 96-well plates were then washed in PBS and resuspended in a final volume of 80 μL fresh PBS. Fluorescence was measured at Ex 495nm / Em 529nm using a microplate reader (Tecan Infinite M200 Pro) and background fluorescence levels consisting of blank wells containing only DCF-DA in PBS subtracted. These experiments were repeated three times and data expressed as mean fold-change ± SEM.

siRNA transfection

MCF-7 cells were seeded at either 7000 cells / well on 96-well plates for MTT assays, 250,000 cells / well on 6-well plates for harvesting RNA for qPCR analysis, or 1,000,000 cells / 6cm dish for harvesting protein for performing immunoblotting. Cells were incubated for 16h following seeding. Cell densities were optimized so that cells reached 50-70% confluency just prior to transfection with siRNA. All cells were transfected with siRNA using Lipofectamine RNAiMax transfection reagent (Life Technologies) according to the manufacturer's instructions for performing a 'forward transfection'. Briefly, cell culture media was removed from cells prior to transfection and replaced with serum-free OptiMEM (Life technologies) cell culture medium. siRNA was firstly diluted in a small volume of OptiMEM equivalent to 10% of the final volume of cells and incubated at RT for 5 min. In parallel, Lipofectamine was diluted in a small volume OptiMEM equivalent to 10% of the final volume of cells and incubated at RT for 5 min. The diluted oligonucleotides and Lipofectamine were then combined and mixed gently, and then incubated at RT for 10min. The siRNA-Lipofectamine complexes formed were added to cells, which were incubated at 37^{o}C for 24 h. The final concentration of siRNA was 50nM and the final amount of Lipofectamine was 0.2% v/v for all experiments. Cells were either transfected with TIGAR siRNA (Silencer Select pre-designed annealed human oligonucleotide duplex; s32680; Life Technologies),

scrambled siRNA (Silencer Select negative control number 2; Life Technologies) or vehicle alone. Following transfection, cells were either harvested for total RNA extraction (as above); harvested for whole protein extraction (as above); or fresh culture media was added and cells were dosed with 8PC6 for 24 h and then an MTT assay performed (as above).

Quantitative RT-PCR

Total RNA was extracted from MCF-7 cells transfected with either TIGAR siRNA or scrambled siRNA using RNeasy Mini Kit (QIAGEN) and quantified using a Nanodrop ND-1000 spectrophotometer. Complementary DNA was synthesised in a 20 µl reaction containing 1 µg of total RNA, using iScript™ cDNA synthesis kit (Bio-Rad) according to the manufacturer's instructions. Quantitative real-time PCRs were performed using Universal Taqman PCR master mix (Applied Biosystems) and the TIGAR (C12orf15; Hs00608644_m1) Taqman Gene Expression Assay (Applied Biosystems) on a CFX Connect Real-Time PCR system (Bio-Rad). Fold change for each experiment was calculated and normalized using the geometric mean of the expression of 18S and Beta-actin. Mean values for fold change ± SEM are given.

Protein immunoblotting

Cells were washed with ice-cold PBS and harvested on ice. Cells were lysed by incubation on ice for 15 min with radioimmunoprecipitation assay (RIPA) buffer (50 mM Tris [pH 7.4], 150 mM NaCl, 10% [v/v] sodium-deoxycholate, 10% [v/v] IGEPAL CA-630; Sigma) containing protease inhibitor cocktail. Lysates were sonicated for 1 min in a sonicating water bath and then centrifuged at 10,500 rpm for 10 min at 4^{o}C. The protein concentration in the supernatant was quantified by the Bradford assay. Proteins were separated on SDS-polyacrylamide Bis-Tris gels under denaturing conditions, transferred to unsupported pure nitrocellulose membrane (Amersham), and subjected to immunoblot analysis.
A mouse monoclonal primary antibody raised against TIGAR (9C10; 1:100; Santa Cruz) was used for blotting. Antibodies were diluted in phosphate-buffered saline containing 5% non-fat powdered milk and 0.1% Tween 20, and incubated with the membrane overnight at 4^{o}C. Horseradish peroxidase-conjugated anti-mouse immunoglobulin G antibody (NXA931, 1:4000; GE Healthcare) was used as the secondary antibody, and monoclonal anti-b-actin-peroxidase antibody (A3854, 1:50,000; Sigma) served as a loading control. Bound immunocomplexes were detected using ECL prime western blot detection reagent (RPN2232; GE Healthcare) and analyzed using Image Lab 4.0 computer software (Bio-Rad). Experiments were repeated three times and a representative blot shown.

Apoptosis assay

MCF-7 cells were seeded at 8 × 10^4 cells/well on 12-well plates and incubated for 16 hours prior to being dosed with different concentrations of 8PC6, as described above. Cells were harvested after 24 hours of drug exposure. This was performed by firstly removing the culture media from the treated cells, which was set aside and later pooled back together with the treated cells, in order to retain any dead, apoptotic and detached cells contained in the spent culture media. Then all remaining adherent cells were gently detached from plates using StemPro Accutase cell dissociation solution (Life Technologies), which helps maintain plasma membrane integrity, and therefore phosphatidylserine (PS) expression. Cells were stained with 7-amino-actinomycin (7-AAD) and FITC-annexin V, using a commercially available FITC-Annexin V Apoptosis Detection Kit (Biolegend, #640922) according to the manufacturer's instructions, with some cell line-specific optimization. Briefly, 7-AAD and FITC-annexin V was diluted in binding buffer at a ratio of 1 in 25 and 1 in 400, respectively, and then added to cell suspensions at a ratio of 1:1. Cells were incubated for 15 minutes at room temperature in the dark with gentle agitation. The stained cells were then analyzed by flow cytometry on an ACEA Novocyte 1000 (ACEA Biosciences Inc.). Percentage of early apoptotic and late apoptotic/necrotic cell populations were calculated using NovoExpress software (version 1.2.1, ACEA Biosciences Inc.) and compared with appropriate controls.

Colony forming assays

MCF-7 cells were seeded in duplicate at 800 cells per dish in 6-cm dishes 16 hr prior to dosing with 8PC6 for 24 hr. Cells were then gently washed in PBS and fresh culture medium added. Cells were cultured for up to 14 days until colonies were visible with fresh medium added every 48–72 hr. At the end of the experiment cells were fixed by addition of methanol/acetic acid (3:1) for 5 min, then stained in 0.5% (v/v) crystal violet solution (diluted in methanol) for 10 min, and colonies counted using the colony area plugin for imageJ. The experiments repeated twice and representative images are shown.

Acknowledgements

This manuscript is dedicated to Dr. Peter Simmonds. The authors thank Professor Adrian Harris and Dr. Karim Bensaad for helpful discussions. This work was funded by Cancer Research UK (Career Establishment Award 10263 to AT), the Engineering and Physical Sciences Research Council (EP/H04986X/1 to AT) and the University of Southampton and A*STAR (Ph.D. studentship for M.G.R. to D.C.H., C.L.L.C. and A.C.).

References

1. Szatrowski TP, Nathan CF. Production of large amounts of hydrogen peroxide by human tumor cells. Cancer Res. 1991;51:794-8.

2. Chen Z, Trotman LC, Shaffer D, Lin HK, Dotan ZA, Niki M, et al. Crucial role of p53-dependent cellular senescence in suppression of Pten-deficient tumorigenesis. Nature. 2005;436:725-30.
3. Hu Y, Rosen DG, Zhou Y, Feng L, Yang G, Liu J, et al. Mitochondrial manganese-superoxide dismutase expression in ovarian cancer: role in cell proliferation and response to oxidative stress. J Biol Chem. 2005;280:39485-92.
4. Radisky DC, Levy DD, Littlepage LE, Liu H, Nelson CM, Fata JE, et al. Rac1b and reactive oxygen species mediate MMP-3-induced EMT and genomic instability. Nature. 2005;436:123-7.
5. Hirota K, Murata M, Sachi Y, Nakamura H, Takeuchi J, Mori K, et al. Distinct roles of thioredoxin in the cytoplasm and in the nucleus. A two-step mechanism of redox regulation of transcription factor NF-kappaB. J Biol Chem. 1999;274:27891-7.
6. Schumacker PT. Reactive oxygen species in cancer cells: live by the sword, die by the sword. Cancer Cell. 2006;10:175-6.
7. Adachi M, Zhang Y, Zhao X, Minami T, Kawamura R, Hinoda Y, et al. Synergistic effect of histone deacetylase inhibitors FK228 and m-carboxycinnamic acid bis-hydroxamide with proteasome inhibitors PSI and PS-341 against gastrointestinal adenocarcinoma cells. Clin Cancer Res. 2004;10:3853-62.
8. Bair JS, Palchaudhuri R, Hergenrother PJ. Chemistry and biology of deoxynyboquinone, a potent inducer of cancer cell death. J Am Chem Soc. 2010;132:5469-78.
9. Lecane PS, Karaman MW, Sirisawad M, Naumovski L, Miller RA, Hacia JG, et al. Motexafin gadolinium and zinc induce oxidative stress responses and apoptosis in B-cell lymphoma lines. Cancer Res. 2005;65:11676-88.
10. Perez-Galan P, Roue G, Villamor N, Montserrat E, Campo E, Colomer D. The proteasome inhibitor bortezomib induces apoptosis in mantle-cell lymphoma through generation of ROS and Noxa activation independent of p53 status. Blood. 2006;107:257-64.
11. Raj L, Ide T, Gurkar AU, Foley M, Schenone M, Li X, et al. Selective killing of cancer cells by a small molecule targeting the stress response to ROS. Nature. 2011;475:231-4.
12. Trachootham D, Zhou Y, Zhang H, Demizu Y, Chen Z, Pelicano H, et al. Selective killing of oncogenically transformed cells through a ROS-mediated mechanism by beta-phenylethyl isothiocyanate. Cancer Cell. 2006;10:241-52.
13. Yang WS, SriRamaratnam R, Welsch ME, Shimada K, Skouta R, Viswanathan VS, et al. Regulation of ferroptotic cancer cell death by GPX4. Cell. 2014;156:317-31.
14. Huang P, Feng L, Oldham EA, Keating MJ, Plunkett W. Superoxide dismutase as a target for the selective killing of cancer cells. Nature. 2000;407:390-5.
15. Pettit GR, Collins JC, Knight JC, Herald DL, Nieman RA, Williams MD, et al. Antineoplastic agents. 485. Isolation and structure of cribrostatin 6, a dark blue cancer cell growth inhibitor from the marine sponge Cribrochalina sp. J Nat Prod. 2003;66:544-7.
16. Hoyt MT, Palchaudhuri R, Hergenrother PJ. Cribrostatin 6 induces death in cancer cells through a reactive oxygen species (ROS)-mediated mechanism. Invest New Drugs. 2011;29:562-73.
17. Knueppel D, Martin SF. Total synthesis of cribrostatin 6. Angew Chem Int Ed Engl. 2009;48:2569-71.
18. Knueppel D, Martin SF. Tandem Electrocyclic Ring Opening/Radical Cyclization: Application to the Total Synthesis of Cribrostatin 6. Tetrahedron. 2011;67:9765-70.
19. Markey MD, Kelly TR. Synthesis of cribrostatin 6. J Org Chem. 2008;73:7441-3.

20. Mohamed M, Goncalves TP, Whitby RJ, Sneddon HF, Harrowven DC. New insights into cyclobutenone rearrangements: a total synthesis of the natural ROS-generating anti-cancer agent cribrostatin 6. Chem Eur J. 2011;17:13698-705.
21. Nakahara S, Kubo A, Mikami Y, Ito J. Synthesis of cribrostatin 6 and its related compounds. Heterocycles. 2006;68:515-20.
22. Packard E, Pascoe DD, Maddaluno J, Goncalves TP, Harrowven DC. Organoytterbium ate complexes extend the value of cyclobutenediones as isoprene equivalents. Angew Chem Int Ed Engl. 2013;52:13076-9.
23. Keston AS, Brandt R. The Fluorometric Analysis of Ultramicro Quantities of Hydrogen Peroxide. Anal Biochem. 1965;11:1-5.
24. Bensaad K, Tsuruta A, Selak MA, Vidal MN, Nakano K, Bartrons R, et al. TIGAR, a p53-inducible regulator of glycolysis and apoptosis. Cell. 2006;126:107-20.
25. Zafarullah M, Li WQ, Sylvester J, Ahmad M. Molecular mechanisms of N-acetylcysteine actions. Cell Mol Life Sci. 2003;60:6-20.
26. Chandel NS, Maltepe E, Goldwasser E, Mathieu CE, Simon MC, Schumacker PT. Mitochondrial reactive oxygen species trigger hypoxia-induced transcription. Proc Natl Acad Sci U S A. 1998;95:11715-20.